Robust design optimization of a photovoltaic-battery-heat pump system with thermal storage under aleatory and epistemic uncertainty

Diederik Coppitters[a,b,c,*], Ward De Paepe[a], Francesco Contino[d]

[a] *Thermal Engineering and Combustion Unit, University of Mons (UMONS), Place du parc 20, 7000 Mons, Belgium*
[b] *Fluid and Thermal Dynamics (FLOW), Vrije Universiteit Brussel, Pleinlaan 2, 1050 Brussels, Belgium*
[c] *Combustion and Robust Optimization Group (BURN), Vrije Universiteit Brussel (VUB) and Université Libre de Bruxelles (ULB), 1050 Brussels, Belgium*
[d] *Institute of Mechanics, Materials and Civil Engineering (iMMC), Université catholique de Louvain (UCLouvain), Place du Levant, 2, 1348 Louvain-la-Neuve*

Abstract

Combining photovoltaic arrays with batteries, heat pumps and thermal storage further decarbonizes the heating sector. When evaluating the performance of such systems, the parameters are either fixed, or based on generic ranges, or characterized by precise distributions inferred from limited information. These assumptions result in suboptimal designs, for which the actual performance differs drastically from simulations. To address these limitations, we consider the effects of limited information (epistemic uncertainty) on the natural variability (aleatory uncertainty) through probability-boxes. First, we performed a robust design optimization on the natural variability of the levelized cost of exergy, followed by a sensitivity analysis on the effects of limited information on the optimized designs. This paper provides the least-sensitive designs to natural variability and effective actions to reduce the effects of limited information. The results indicate that a photovoltaic-battery-heat pump configuration achieves higher robustness towards aleatory uncertainty than a photovoltaic-battery-gas boiler configuration. To determine the true-but-unknown performance and ro-

*Corresponding author
Email address: diederik.coppitters@umons.ac.be (Diederik Coppitters)

bustness of the optimized designs, clarifying the grid electricity contract and adopting specific energy demand profiles are the main actions, while considering generic technology models contributes little to the epistemic uncertainty.
Keywords: Aleatory uncertainty; epistemic uncertainty; heat pump; probability-box; robust design optimization; thermal energy storage.

---

1. Introduction

Distributed solar PhotoVoltaic (PV) capacity is expected to nearly triple its capacity growth between 2019 and 2024 (406 GW) as opposed to 2012-2018 (142 GW) [1]. To handle the intermittent PV energy supply, this growth of distributed PV capacity appeals for improved power system flexibility [2]. Among others, the market expansion of electrical energy storage [3] and thermal energy storage [4] enables greater power system flexibility. To illustrate, Murugan et al. [5] reviewed polygeneration systems that combine power and heating with other energy streams, such as cooling and synthetic fuels. Kyriakarakos et al. [6] evaluated a PV capacity in a polygeneration microgrid with a bank of batteries, a hydrogen-based energy system and a reverse osmosis desalination unit. Rad et al. [7] integrated a PV capacity in a hybrid power system with wind turbines, a biogas generator and a fuel cell. In the residential sector, battery technology provides a flexible, adequate technology for short-term (i.e. days) electrical energy storage to improve PV self-consumption [8]. In addition to battery energy storage, including heat pumps and thermal storage to cover the heat demand further improves the PV self-consumption and entails the coupling of the electricity sector and heating sector [9, 10], which is anticipated to further decarbonize the heating sector [3]. Several studies evaluated the feasibility of a PV-battery-heat pump system in the residential sector [11]. Klinger evaluated the PV and battery market potential in combination with heat pumps and electric vehicles and concluded that households benefit from such a self-consuming system [12]. Angenendt et al. [13] evaluated the profitability of the participation of a residential PV-battery-heat pump system in the frequency

Nomenclature

A	area, m^2	RDO	Robust Design Optimization
$a, ..., d$	compression efficiency coefficients	r_p	compression ratio
C	capacity, Ah	s	entropy, kJ/(kg K)
$CAPEX_a$	annual capital expense, €	SOC	State Of Charge
$C_{e,a}$	annual grid electricity cost, €	T	temperature, K
$C_{g,a}$	annual gas cost, €	U	voltage, V
COP	Coefficient Of Performance	U_{loss}	heat loss coefficient, $1\,W/(m^2K)$
$C_{r,a}$	annual replacement costs, €	UQ	Uncertainty Quantification
CRF	Capital Recovery Factor	X	exergy, MWh
F	Carnot coefficient	η	efficiency
f	inflation rate	μ	mean
h	enthalpy, kJ/kg	σ	standard deviation
i	annualized interest rate	Ψ	orthogonal polynomial
i'	nominal interest rate	amb	ambient
I	current, A	bat	battery
K_0, K_1, K_2	conversion power coefficients	c	condensing
L	system lifetime, year	ch	charge
LCOX	Levelized Cost Of eXergy, €/MWh	dch	discharge
M	stochastic dimension	e	evaporation
N_{bat}	battery capacity, kWh	L	photogenerated
N_{hp}	heat pump capacity, kW_{th}	nom	nominal
N_{PV}	photovoltaic array capacity, kW_p	oc	open-circuit
$N_{thermal\ storage}$	thermal storage capacity, l	pinch	pinch
$OPEX_a$	annual operational expense, €	sh	shunt
p	polynomial order	s	series
PV	PhotoVoltaic	th	thermal
Q	heat, kJ	w	water
R	resistance, Ω		

control reserve market. Despite the increased battery ageing, this approach was proven profitable following the ability to convert negative control reserve power

into residential heating. Angenendt et al. [14] evaluated the sizing of a PV array, bank of batteries, heat pump and thermal storage for a household under different operating strategies and concluded that small-scale energy storage is economically beneficial.

In such design and feasibility studies, several techno-economic parameters determine the performance of a PV-battery-heat pump configuration. These parameters are often assumed deterministic and therefore correspond to a specific scenario. However, the system performance is affected by uncertainty, e.g. through variable market conditions, occupant behaviour on energy consumption and interannual variability of solar irradiance. Consequently, this uncertainty should be considered in design and feasibility studies to shape the stochastic space under which decisions should be taken [15]. In the rare case of considering uncertainty in renewable energy system optimization [16], the uncertainties were characterized through precise distributions [17] or generic ranges [18]. Wakui et al. [19] considered multiple forecasting scenarios on the model parameters in a combined two-stage stochastic schedule programming and rule-based control on a residential PV-battery-heat pump system, which proves beneficial over a deterministic alternative by taking advantage of historical PV output, by using PV output for the heat pump during daytime and by battery discharging during high grid electricity prices. However, the construction of such precise probability distributions is ambiguous for some variables due to limited knowledge, resulting in biased conclusions from the stochastic performance analysis [20].

To characterize the uncertainty on a parameter for which the precise distribution is inferred from limited information, imprecise probabilities are considered [21]. In imprecise probability theory, the uncertainty following from limited knowledge (i.e. epistemic uncertainty) and the uncertainty from natural variation (i.e. aleatory uncertainty) are categorized separately [22]. As knowledge or the amount of data can be improved, epistemic uncertainty is considered reducible (e.g. specifying the PV type as opposed to a generic model). Aleatory uncertainty represents the natural variability of the parameter and is there-

fore irreducible (e.g. future natural gas price). In an energy system framework, Moret et al. [23] provided a clear description of the epistemic and aleatory uncertainty on energy system parameters. Among the imprecise probability characterization methods, parametric probability boxes (p-boxes) provide an intuitive representation of mixed epistemic and aleatory uncertainty on model parameters [20].

Characterizing the uncertainty on the parameters at the model input with probability boxes complicates the uncertainty propagation. While for precise distributions, Uncertainty Quantification (UQ) methods are well-established (e.g. Monte Carlo Simulation [24], Gaussian Process Regression [25] and Polynomial Chaos Expansion (PCE) [26]), UQ applications in an imprecise probability context are rare and often rely on a computationally expensive (i.e. $> 10^6$ evaluations) nested Monte Carlo Simulation [27]. Recently, Schöbi et al. [27] proposed an augmented PCE which enables to propagate probability boxes and quantify the Sobol' indices (i.e. global sensitivity indices) in a computationally efficient manner.

Once the stochastic performance of a system is determined, the stochastic moments can be used as design optimization objectives. In Robust Design Optimization (RDO) with precise probabilities, the standard deviation is minimized to provide designs least-sensitive to its random environment [28]. A typical RDO case study is the optimization of the node displacement through the design of the cross-sectional areas of a four-bar truss [29]. The design with the optimized displacement mean of 3.84 mm is subject to a displacement standard deviation of 0.40 mm, while the robust design achieves a displacement mean of 3.97 mm and a displacement standard deviation of 0.18 mm. This alternative robust design is beneficial, as the design is significantly less sensitive to the random environment, while the increase in displacement mean is limited. Several applications exist of RDO on energy systems. De Paepe et al. [30] provided a robust design for a micro gas turbine by minimizing the relative standard deviation of the electrical efficiency and power output. Despite that the micro gas turbine is rather insensitive to the technical uncertainties, the robustness can be

improved by reducing the rotational speed and operating near the turbine outlet temperature upper limit. The authors of this paper performed RDO on the levelized cost of electricity of a PV-battery-hydrogen system [31]. The results illustrate that considering a photovoltaic array without energy storage results in the optimized levelized cost of electricity mean, while considering battery storage and hydrogen storage improves the robustness. In an imprecise probability framework, stochastic optimization applications are scarce [32]. Xie et al. [33] performed an RDO by considering the standard deviation of the upper-limit Cumulative Density Function (CDF), to guarantee safe operation.

This paper provides the optimized stochastic designs (including the robust design) and effective actions to reduce the effects of limited information on the Levelized Cost Of eXergy (LCOX) for a residential PV-battery-heat pump system. By characterizing the effects of limited information (epistemic uncertainty) and natural variability (aleatory uncertainty) through probability-boxes, the work addresses the limitation of using deterministic parameters or scenarios, which can lead to biased designs and unwarranted actions to reduce performance variation. Thereafter, we aimed at minimizing the effect of aleatory uncertainty on the LCOX through a surrogate-assisted RDO. Hence, this approach determines the designs least-sensitive towards the irreducible aleatory uncertainty. Finally, we performed a global sensitivity analysis on the optimized designs to quantify the significance of epistemic uncertainty on the predicted performance and robustness of the optimized designs, followed by guidelines to reduce the epistemic uncertainty effectively.

In this paper, the system model, uncertainty characterization and RDO method are described in section 2. The optimized designs and the global sensitivity analysis are presented in section 3. The conclusion and main messages of the work are summarized in section 4.

2. Method

In this section, the system is described and the optimization criteria are introduced. Thereafter, the uncertainty characterization through precise and imprecise probabilities is illustrated, followed by the UQ method that propagates the uncertainties and quantifies the statistical moments and Sobol' indices. The section concludes with the surrogate-assisted RDO structure.

2.1. System model

In this work, we consider a grid-connected dwelling in Brussels, Belgium. The climate data for Brussels and the electricity and heat demand for the household are discussed in subsection 2.2. This household is supported by a PV array, which is primarily used to cover the electricity demand of the household (i.e. electric appliances, lighting and cooking). To cover the heat demand of the dwelling (i.e. Space Heating (SH) and Domestic Hot Water (DHW)), we consider two different technologies: a gas boiler, sized to cover the entire heat demand and connected to the natural gas grid (Figure 1), and an Air-Source Heat Pump (ASHP), connected to a thermal storage tank with an electric heater (Figure 2). The communication between the components and the monitoring of the energy system is performed by a programmable logic controller [34].

In both systems, PV electricity is used to cover the electricity demand. When excess PV electricity is available, the electricity is stored in the bank of batteries when considering the gas boiler, while the PV excess electricity is used to power the ASHP before storing the electricity in the bank of batteries in the PV-battery-ASHP configuration. Inversely, when the electricity demand exceeds the PV electricity, the bank of batteries is called upon first, followed by the grid whenever necessary.

To cover the DHW and SH demand, heat is supplied either by the gas boiler at an efficiency of 90 % [35] or extracted from the thermal storage tank. When the stored thermal energy is insufficient, the ASHP is used to comply with the remaining heat demand. If the PV excess electricity is insufficient to

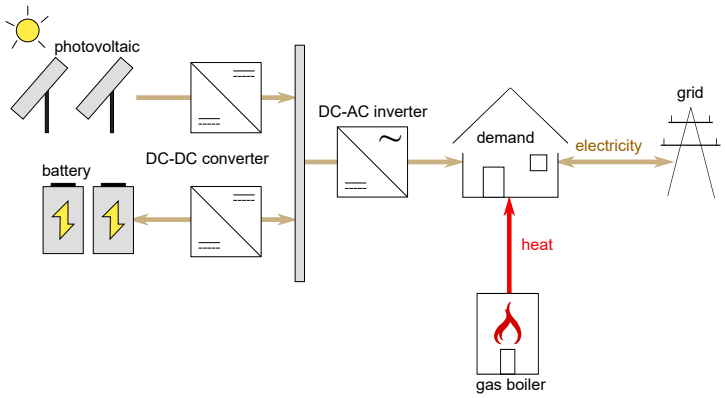

Figure 1: The reference system consists of a photovoltaic array and bank of batteries, which operate in support of the electricity grid to cover the electricity demand. A natural gas boiler covers the heat demand.

run the ASHP, two power management strategies are considered to cover the remaining required electricity for the ASHP. In the first strategy, electricity from the grid is adopted (i.e. PV-battery-ASHP without battery support). Hence, the stored excess of PV electricity in the battery is only used to cover the electricity demand, which is considered high-quality energy. In the second strategy, the electricity stored in the battery is used to run the ASHP, before covering the electricity demand (i.e. PV-battery-ASHP with battery support). This strategy enables to run the ASHP with renewable electricity when the solar irradiance is insufficient (e.g. at night) and therefore reduces the grid electricity consumption. In both power management strategies, a grid-powered, back-up electric heater is considered with a fixed 99% efficiency [36]. The back-up electric heater is deployed to support the ASHP and thermal storage capacity to cover demand peaks [37], which ensures thermal comfort in the household.

2.1.1. Photovoltaic array

To model the PV array performance, we imported the open-source *PVlib* Python package [38]. The *PVlib* package is validated with experimental data and with results from existing commercial software [39]. The single-diode model

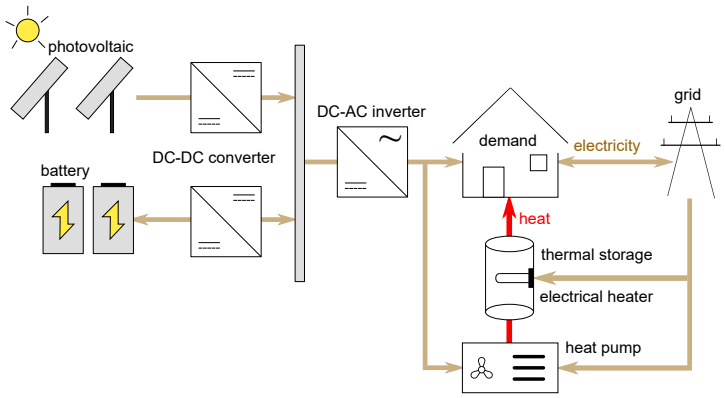

Figure 2: The photovoltaic-battery-heat pump system consists of a photovoltaic array that primarily complies with electricity demand. Excess photovoltaic electricity is used to power the heat pump, which is used to heat the water in the thermal storage tank to comply with the domestic hot water and space heating demand. The grid is used as a back-up power generator to comply with electricity demand, to run the heat pump and to supply the electric heater.

provides the PV current and voltage:

$$I_{\mathrm{PV}} = I_{\mathrm{L}} - I_0 \left(\exp\left(\frac{U + IR_{\mathrm{s}}}{n_{\mathrm{diode}} N_{\mathrm{s}} U_{\mathrm{th}}} \right) - 1 \right) - \frac{U + IR_{\mathrm{s}}}{R_{\mathrm{sh}}}. \tag{1}$$

In this model, the parameters are determined based on manufacturer data, through the method developed by De Soto et al. [40]. The manufacturer data is adopted from a typical monocrystalline silicon PV panel (Sunpower SPR X-19-240-BLK, 240 $\mathrm{W_p}$ nominal power, 5 % power tolerance, 42.8 V rated voltage, 5.61 A rated current, 50.6 V open-circuit voltage and 5.98 A short-circuit current) [41]. The resulting current-voltage characteristic provides the power output in function of the solar irradiance and ambient temperature. As the PV array is connected to a DC-DC converter with Maximum Power Point Tracking, the maximum power point is assumed as the operating point at each time step. At this maximum power point, the efficiency of the PV technology is approximately 19.3 % in a typical solar irradiance range of 250 $\mathrm{W/m^2}$ - 1000 $\mathrm{W/m^2}$, with a maximum efficiency of 19.4 % near a solar irradiance of 580 $\mathrm{W/m^2}$ (Figure 3).

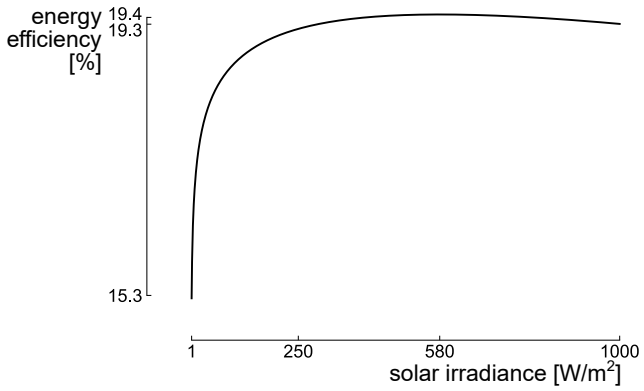

Figure 3: The energy efficiency of the considered photovoltaic technology in function of the solar irradiance illustrates that the efficiency is near 19.3 % in a typical solar irradiance range of 250 $\mathrm{W/m^2}$ - 1000 $\mathrm{W/m^2}$.

2.1.2. Bank of batteries

To simulate the battery electricity storage, the widespread and mature lead-acid battery technology is adopted [42]. Alternatively, lithium-ion batteries promise higher power, energy density and a significant market share in the future. However, the installation experience and availability are limited [42]. Moreover, in the context of this work, the larger uncertainty on cost and operation is a significant drawback as opposed to the well-defined lead-acid battery technology [43].

The voltage-current characteristic of lead-acid battery technology is adopted from the experimentally-validated model of Blaifi et al. [44]:

$$U_{\mathrm{bat}} = U_{\mathrm{bat,oc}} + I_{\mathrm{bat}} R_{\mathrm{bat}}, \tag{2}$$

where the battery current I_{bat} is positive during charge and negative during discharge. The resistance component R_{bat} determines the voltage evolution after charging and discharging and depends, among others, on temperature, current magnitude and capacity [44]. The charge and discharge voltage are

quantified as follows:

$$U_{\mathrm{ch}} = (2.085 - 0.12\,(1 - \mathrm{SOC})) - \frac{I}{C_{nom}} \left(\frac{4}{1 + I^{1.3}} + \frac{0.27}{\mathrm{SOC}^{1.5}} + 0.02 \right) (1 - 0.007\Delta T)\,, \tag{3}$$

$$U_{\mathrm{dch}} = (2 - 0.16\ \mathrm{SOC}) + \frac{I}{C_{nom}} \left(\frac{6}{1 + I^{0.86}} + \frac{0.48}{(1 - \mathrm{SOC})^{1.2}} + 0.036 \right) (1 - 0.025\Delta T)\,. \tag{4}$$

While the nominal capacity is fixed, the instantaneous capacity (i.e. the amount of useful charge) depends on the operating temperature and the discharged current:

$$C = \frac{1.67 C_{\mathrm{nom}}}{1 + 0.67 \left(\dfrac{I}{I_{\mathrm{nom}}} \right)^{0.9}} (1 + 0.005\Delta T)\,. \tag{5}$$

The State Of Charge (SOC) represents the relative amount of electricity stored:

$$\mathrm{SOC}\,(t) = \mathrm{SOC}_0 + \frac{1}{C\,(t)} \int_0^t \eta_{\mathrm{bat}}\,(t)\, I\,(t)\, \mathrm{d}t, \tag{6}$$

for which the minimum SOC is assumed at 20 % [43, 45]. Additional technical characteristics are described by Blaifi et al. [44]. The SOC determines the Depth Of Discharge ($= 1 - \mathrm{SOC}$), which affects the battery lifetime in addition to the charge current, discharge current, overcharging and over-discharging. Considering these parameters, the battery lifetime is determined through the Rainflow cycles counting method [46]. However, to avoid excessive reduction of the battery lifetime during system operation, overcharging and over-discharging are avoided and the maximum charge current and maximum discharge current are limited to $C_{\mathrm{nom}}/10$ and $C_{\mathrm{nom}}/3.3$, respectively [47].

2.1.3. Air Source Heat Pump

The heat pump is an air-to-water, on/off-controlled heat pump, which uses ambient air as a heat source and R410A as a working fluid. The heat pump

is modelled following a refrigeration cycle, in which pressure losses, evaporator superheating and condensing subcooling are neglected [48]. A pinch temperature T_{pinch} of 5 K is selected, which results in the following condensing temperature T_{c} and evaporation temperature T_{e}:

$$T_{\text{c}} = T_{\text{w}} + T_{\text{pinch}}, \tag{7}$$

$$T_{\text{e}} = T_{\text{amb}} - T_{\text{pinch}}. \tag{8}$$

To reach the condensing temperature after evaporation, the air is compressed in a compressor unit. As the compressor inlet pressure depends on the ambient temperature, the compression ratio is variable during the ASHP system lifetime. To determine the effect of the variable compression ratio on the compression isentropic efficiency, we adopted the experimentally-validated model from Underwood et al. [48]:

$$\eta_{\text{comp,is}} = \frac{a\ \exp\left(-b\left(r_p - c\right)\right)}{1 + \exp\left(-d\left(r_p - c\right)\right)}, \tag{9}$$

where the coefficients $a, ..., d$ are fitted based on manufacturer data [48]. The compression ratio r_p is determined through the pressure at which the condensation and evaporation occurs. These pressures are characterized by the respective refrigeration properties, extracted from the CoolProp Python library. The compressor specific work is then quantified as follows:

$$\Delta h_{\text{comp}} = \frac{h\left(p_{\text{c}}, s_{\text{comp,in}}\right) - h_{\text{comp,in}}}{\eta_{\text{comp,is}}}. \tag{10}$$

Following the characterization of the enthalpy after condensation $h_{\text{c,out}}$, the heat generation during condensation Q_{c} and Coefficient Of Performance (COP) are determined:

$$Q_{\text{c}} = \dot{m}\left(h_{\text{comp,out}} - h_{\text{c,out}}\right), \tag{11}$$

$$\mathrm{COP} = \frac{Q_\mathrm{c}}{\dot{m}\Delta h_\mathrm{comp}}. \tag{12}$$

At 10.4 °C ambient temperature (i.e. the average annual ambient temperature adopted for Brussels, see Table A.3), the COP is 3.1, which corresponds to the experimentally-validated value presented by Angenendt et al. [14].

2.1.4. Thermal storage tank

The stratified thermal storage tank is a DHW and SH combisystem with a heat exchanger that separates the drinking water from the heating water. Considering the DHW temperature of 40 °C and the heat pump limits, the lower and upper temperature are set at 45 °C and 55 °C, respectively [14]. The SH demand depends on the ambient temperature, room temperature and building losses. In this work, the SH (and DHW) demand is characterized by an energy demand profile, which represents the heat required to reach the required space temperature under the specific conditions. Hence, the demand is characterized by the energy demand per hour, which is extracted from the thermal storage tank. The heat loss of the storage tank is determined through the room temperature T_room and the natural convection heat exchange coefficient (i.e. heat loss coefficient) U_loss [14]:

$$Q_\mathrm{loss} = U_\mathrm{loss} A_\mathrm{tank} \left(T_\mathrm{w,tank} - T_\mathrm{room}\right), \tag{13}$$

where the room temperature T_room is assumed constant at 20 °C and the heat loss coefficient U_loss is assumed at 1 W/(m^{2}K) [14].

2.1.5. Power converters and inverter

The DC-AC inverter connects the PV array and bank of batteries with the household and heat pump. The AC output power depends on the inverter efficiency $\eta_\mathrm{inv}\left(P_\mathrm{AC,out}\right)$:

$$P_\mathrm{AC,out} = \eta_\mathrm{inv}\left(P_\mathrm{AC,out}\right) P_\mathrm{DC,in}. \tag{14}$$

To quantify the varying efficiency in function of the operating point, the inverter efficiency is determined through experimentally-validated power coefficients K_0, K_1, K_2 [49]:

$$\eta_{\text{inv}} = \frac{P_{\text{AC}}/P_{\text{nom}}}{P_{\text{AC}}/P_{\text{nom}} + K_0 + K_1 P_{\text{AC}}/P_{\text{nom}} + K_2 \left(P_{\text{AC}}/P_{\text{nom}}\right)^2}, \tag{15}$$

where the power coefficients are adopted from the SMA Sunny Boy 700U [49]. The PV array and bank of batteries are connected to a DC bus bar through DC-DC converters. The power conversion is quantified similar to the DC-AC power conversion:

$$P_{\text{DC,out}} = \eta_{\text{conv}} \left(P_{\text{DC,out}}\right) P_{\text{DC,in}}, \tag{16}$$

where $P_{\text{DC,out}}$ corresponds to the converter output power. The conversion efficiency profiles are adopted from Taghvaee et al. [50], for which a buck-boost converter and a bidirectional buck-boost converter are selected for the PV array and a bank of batteries, respectively.

2.2. Climate and demand data

The energy consumption of the grid-connected household depends on the solar irradiance, ambient temperature, electricity demand and heating demand of the household (Figure 4). Therefore, these climate conditions and demand profiles are adjusted to the specific location (Brussels) and demand (dwelling). As the energy demand of the household is affected by the weather (i.e. SH demand correlates to the ambient temperature and solar irradiance), the analysis should be conducted with climate data that corresponds to the energy demand profiles. Therefore, we adopt the Typical Meteorological Year data and hourly energy demand data (electricity, SH and DHW) provided by the National Renewable Energy Laboratory, as the former is used to construct the latter [51, 52]. To adapt the climate and demand profiles to Belgium and its average household energy consumption, we implemented the method from Montero Carrero et al. [53]. The electricity demand profile combines the different loads of the dwelling

(i.e. electric appliances, lighting and cooking). Therefore, in this work, no details are available on the contribution of each electric load to the hourly overall electricity demand. The SH period is specified based on the monthly average ambient temperature and aims to ensure thermal comfort [54]: when the monthly average temperature is less than 19 °C, the heating system is enabled for that month. Consequently for Brussels, the SH is considered for the entire year.

2.3. Design parameters and objective

The system is designed by sizing the components of the system, i.e. the capacity of the PV array, bank of batteries, ASHP and thermal storage tank. By considering these capacities as independent design parameters, the optimization algorithm can exclude any technology from the design (e.g. no thermal storage tank). The quantity of interest is the Levelized Cost Of eXergy (LCOX). In this quantity of interest, exergy is selected to account for the true quality of both energy streams in one metric [55]. Hence, the LCOX reflects the system cost per unit of exergy covered [45]:

$$\mathrm{LCOX} = \frac{\mathrm{CAPEX_a} + \mathrm{OPEX_a} + C_{\mathrm{r,a}} + C_{\mathrm{e,a}} + C_{\mathrm{g,a}}}{X_{\mathrm{demand}}}. \tag{17}$$

To determine the annual system cost, the annualized investment cost $\mathrm{CAPEX_a}$, operational cost $\mathrm{OPEX_a}$, replacement cost $C_{\mathrm{r,a}}$, grid electricity cost $C_{\mathrm{e,a}}$ (and gas cost $C_{\mathrm{g,a}}$ when a gas boiler is considered) are added together. $\mathrm{CAPEX_a}$ represents the annualized capital expenses for every system component [45]:

$$\mathrm{CAPEX_a} = \mathrm{CRF} \sum_{k=0}^{c} N_k \mathrm{CAPEX}_k, \tag{18}$$

where c refers to the different components (i.e. PV array, battery bank, thermal storage tank, heat pump, gas boiler, DC-DC converters and DC-AC inverter) and N represents the corresponding installed capacity. The Capital Recovery Factor (CRF) is determined by the annualized interest rate i and the system

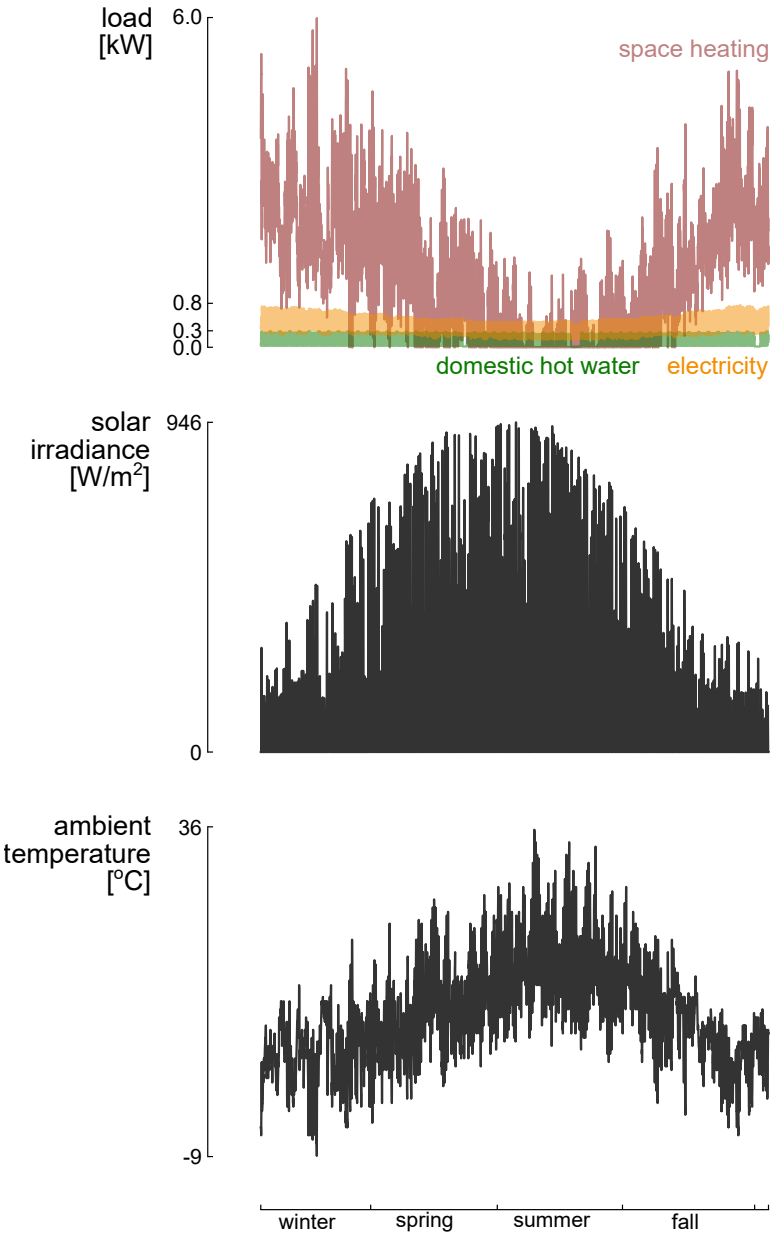

Figure 4: The hourly solar irradiance, ambient temperature and energy demand (electricity, domestic hot water and space heating) profiles for Brussels show that the energy demands drop during spring and summer and increase during fall and winter.

lifetime L (20 years):

$$\mathrm{CRF} = \frac{i(1+i)^L}{(1+i)^L - 1}. \tag{19}$$

The annualized interest rate considers the effect of inflation f on the initial interest rate at the moment of loan i':

$$i = \frac{i' - f}{1+f}. \tag{20}$$

In addition to the investment cost, the system is subject to costs related to the component operation and maintenance. The annualized operating expenses are quantified through [45]:

$$\mathrm{OPEX_a} = \sum_{k=0}^{c} N_k \mathrm{OPEX}_k. \tag{21}$$

The system components come with different lifetimes. Consequently, some components might need replacement during the system lifetime, which induces additional cost. The annualized replacement cost is described as [45]:

$$C_{\mathrm{r,a}} = \mathrm{CRF} \sum_{k=0}^{c} \left(N_k R_{\mathrm{c,k}} \sum_{l=0}^{r_k} (1+i)^{-lt_k} \right), \tag{22}$$

where r_k is the number of replacements during the system lifetime for every component and t_k is the replacement period. Finally, when the system is unable to cover part of the load (SH, DHW and electricity), electricity (and gas when considering the gas boiler) is extracted from the grid. As a result, additional costs are included which relate to the electricity price (and gas price). In this work, a fixed annual electricity tariff is adopted, which corresponds to the contract of nearly 75% of the households in Belgium [56].

The annual exergy output X_{demand} is characterized by the sum of the annual exergy required for electricity (elec), DHW and SH [57]:

$$\sum_{i=1}^{8760} \sum_{\mathrm{type}} X^{\mathrm{type}}, \qquad \mathrm{type} \in \{\mathrm{elec}, \mathrm{DHW}, \mathrm{SH}\}. \tag{23}$$

While the electricity demand is covered by the highest energy quality, i.e. $X^{\text{elec}} = E^{\text{elec}}$, the exergy to cover the DHW demand and SH demand are scaled by their corresponding Carnot coefficient F [57]:

$$X^{\text{type}} = F^{\text{type}} E^{\text{type}} \qquad \text{type} \in \{\text{DHW}, \text{SH}\}, \tag{24}$$

$$F = 1 - \frac{T_{\text{ref}}}{T_{\text{req}}}, \tag{25}$$

where the reference temperature T_{ref} corresponds to the ambient temperature for each specific hour of the year and T_{req} corresponds to the temperature required for DHW and SH, set at 40 °C and 35 °C, respectively [14].

2.4. Uncertainty characterization

The uncertainty on a model parameter can be characterized as epistemic uncertainty or aleatory uncertainty. Epistemic uncertainty is the uncertainty related to the lack of knowledge on the parameter, but this knowledge can be improved by gaining more information on the parameter (e.g. in the context of a PV-battery-ASHP system, the epistemic uncertainty on a typical annual electricity demand can come from the unknown occupant behaviour). The epistemic uncertainty can be reduced by adopting an actual annual electricity demand from a specific household. The aleatory uncertainty relates to the unknown evolution of the parameter value and is therefore irreducible. To illustrate, the aleatory uncertainty on wholesale electricity price comes from the unknown evolution of this parameter in the coming years. Both uncertainty types can affect a single model parameter simultaneously. To characterize the effect of both uncertainties on a single stochastic parameter, a parametric probability-box (p-box) is considered. Such a p-box characterizes both uncertainty types for a single stochastic parameter, while maintaining a clear separation between the effect of epistemic and aleatory uncertainty on that parameter [27] (Figure 5). Such a p-box is defined by interval-valued statistical moments: $\mu \in [\mu_{\min}, \mu_{\max}]$, $\sigma \in [\sigma_{\min}, \sigma_{\max}]$. In this formulation, the true-but-unknown mean μ and standard deviation σ are situated in between the respective bounds and represent

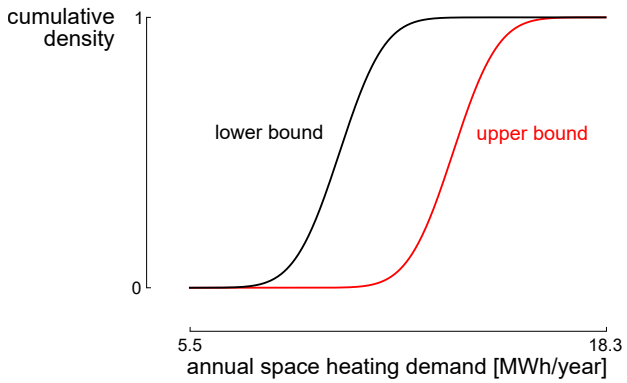

Figure 5: The parametric probability-box (p-box) of the annual space heating demand combines the effect of epistemic uncertainty (i.e. occupant behaviour) and aleatory uncertainty (i.e. future evolution) on the parameter. The true-but-unknown CDF, which lies between the lower bound and upper bound of the p-box and is characterized by a mean and standard deviation, represents the aleatory uncertainty of the space heating demand. The range on the p-box represents the epistemic uncertainty on the parameter and affects the mean and standard deviation.

the aleatory uncertainty. The range on the statistical moments represents the epistemic uncertainty.

In this work, the grid electricity price, natural gas price, electricity demand and heat demand are subjected to both epistemic and aleatory uncertainty and thus characterized by a p-box (Table A.2). For the electricity price, six prediction scenarios are combined to define the aleatory uncertainty, i.e. a base case scenario, a decentral scenario and a large-scale renewable energy system scenario, each determined in the coal-before-gas merit order and gas-before-coal merit order [58]. Similar for the gas cost, where the aleatory uncertainty integrates over low, middle and high gas cost scenarios [59]. The epistemic uncertainty relates to the different energy tariffs available for the household and thus to the different prices for the electricity extracted from the electricity grid (and gas from the gas grid) [60]. Conclusively, the true-but-unknown mean and standard deviation represent the aleatory uncertainty on the future evolution of these prices, while not fixing the energy supplier for the household induces epistemic uncertainty, i.e. the range on the mean value. A similar philosophy is

applied to the electricity demand and heat demand. The uncertainty following the different prediction scenarios for the future evolution of the energy demand represent the aleatory uncertainty [61, 62]. As a typical energy demand is assumed for average household consumption, the epistemic uncertainty is induced by the unknown occupant behaviour [63]. Conclusively, the system performance is subjected to the uncertainty on how the energy demand will evolve (e.g. policies on increased insulation, improving efficiency of electric appliances) and how the occupants behave in their consumption (e.g. heavy consumers or light consumers).

Next to the p-boxes, several parameters are characterized only by aleatory uncertainty (Table A.3). The solar irradiance and ambient temperature are characterized by a Typical Meteorological Year, which is assumed valid over the lifetime of the system. Hence, the epistemic uncertainty is neglected. The aleatory uncertainty corresponds to the interannual variability, which is based on percentiles from historical data [64]. Besides, the inflation rate is characterized by aleatory uncertainty following its natural variation [65].

Finally, the costs related to each technology are characterized by epistemic uncertainty (Table A.4). These parameters are fixed at the beginning of the project and therefore only subject to the lack of knowledge on the market during system design, before making the actual investment.

2.5. Uncertainty quantification

To propagate p-boxes, the nested Monte Carlo Simulation method is computationally intractable. Instead, we adopted the Polynomial Chaos Expansion (PCE) surrogate modelling method presented by Schöbi et al. [27]. To characterize the coefficients of the PCE in a computationally efficient way, we considered the stepwise regression method developed in our research group [66].

In a precise distribution context, a PCE representation $\mathcal{M}^{\mathrm{PCE}}$ of the system model $\mathcal{M}$ for a random vector X with independent components consists of a series of multivariate orthonormal polynomials $\Psi_{\boldsymbol{\alpha}}$ with corresponding coefficients

$u_{\boldsymbol{\alpha}}$ [67]:

$$\mathcal{M}^{\mathrm{PCE}}(\boldsymbol{X}) = \sum_{\boldsymbol{\alpha}\in\mathcal{A}} u_{\boldsymbol{\alpha}} \Psi_{\boldsymbol{\alpha}}(\boldsymbol{X}) \approx \mathcal{M}(\boldsymbol{X}), \tag{26}$$

where $\boldsymbol{\alpha}$ are the multi-indices and $\mathcal{A}$ is the considered set of multi-indices, for which the size is defined by a truncation scheme. A typical truncation scheme is limiting the polynomial order up to a certain degree, which constrains the number of multi-indices in the set to [67]:

$$|\mathcal{A}^{M,p}| = \frac{(p+M)!}{p!M!}, \tag{27}$$

where p corresponds to the polynomial order and $M = |\boldsymbol{X}|$ is the stochastic dimension, i.e. the number of random variables.

When parametric p-boxes are considered, the epistemic and aleatory uncertainty can be separated into two vectors: a vector with independent uniform distributions $\boldsymbol{\Theta}$ (i.e. the interval ranged statistical moments) and a vector with the aleatory uncertainty distributions $\boldsymbol{X}$, respectively [27]. Hence, an augmented input vector ($\boldsymbol{\Theta}$, $\boldsymbol{X}$) becomes the stochastic model input in a parametric p-box context. The augmented input vector components are dependent on each other, i.e. the random value sampled from the aleatory uncertainty $\boldsymbol{X}$ depends on the sampled statistical moments from the epistemic uncertainty $\boldsymbol{\Theta}$. As the PCE input assumes independent random variables, the augmented input vector ($\boldsymbol{\Theta}$, $\boldsymbol{X}$) needs to be mapped into a vector with independent components $\boldsymbol{V}$ through isoprobabilistic transformation [27]. To illustrate, for a Gaussian distribution $X \sim \mathcal{N}(\mu_X, \sigma_X)$ with $\boldsymbol{\theta} = (\mu_X, \sigma_X)$, the isoprobabilistic transform corresponds to:

$$X = \mu_X + \sigma_X \zeta, \tag{28}$$

where ζ is a standard Gaussian variable $\zeta \sim \mathcal{N}(0, 1)$. Then, the independent input vector corresponds to $V = (\zeta, \mu_X, \sigma_X)$, resulting in a dimensionality for the vector $\boldsymbol{V}$ equal to $M_{\mathrm{aug}} = |\boldsymbol{V}| = 3|\boldsymbol{X}|$. After this transformation, the PCE

for parametric p-boxes can be constructed:

$$\mathcal{M}^{\text{aug,PCE}}(\boldsymbol{V}) = \sum_{\boldsymbol{\alpha} \in \mathcal{A}} u_{\boldsymbol{\alpha}} \Psi_{\boldsymbol{\alpha}}(\boldsymbol{V}). \tag{29}$$

As the stochastic parameters in the input vector are considered independent to construct the PCE, the dependency between the uncertainties (i.e. between ambient temperature and space heating demand) is neglected. To compute the coefficients in the PCE, training samples are needed. When adopting Equation 27 to determine the size of the experimental design n, where M is replaced with the stochastic dimension $M^{\text{aug}} = 3M$ for the augmented PCE, the number of samples grow dramatically (i.e. curse-of-dimensionality) [67]. Therefore, we adopted a stepwise regression approach, as proposed by Abraham et al. [66]. In the first forward step of this approach, $|\mathcal{A}^{M^{\text{aug}},p}|$ basis functions (i.e. the orthonormal polynomials) are assessed individually by fitting their response with the model response on the experimental design $V = v^1, v^2, ..., v^n$. Then, for each basis function, a one-predictor regression model (i.e. orthonormal polynomial + coefficient) is solved through Least-Square Minimization. The best performing one-predictor regression model, with the most significant coefficient, is added to the final surrogate model. After each amplification of the surrogate model, a backward step evaluates the confidence interval of the previously entered regression coefficients and removes any coefficient with a confidence interval of zero. This process is repeated until the maximum number of iterations is reached and the fitted residual is minimized. Additional details on this method are described by Abraham et al. [66].

When the PCE is constructed, the interval-ranged mean $[\mu_{\min}, \mu_{\max}]$ and interval-ranged standard deviation $[\sigma_{\min}, \sigma_{\max}]$ are computed through a nested Monte Carlo Simulation on the PCE. The imprecise total-order Sobol' indices, which quantify the total impact (i.e. including mutual interactions) of the aleatory uncertainty for each stochastic input parameter on the performance indicator, can be quantified analytically via the regression coefficients. First, the multi-indices and orthonormal polynomials are decomposed into the multi-indices and

orthonormal polynomials related to the epistemic uncertainty $\boldsymbol{\Theta}$ and aleatory uncertainty $\boldsymbol{X}$, i.e. $\boldsymbol{\alpha} = (\boldsymbol{\alpha_\Theta}, \boldsymbol{\alpha_X})$ and $\Psi_{\boldsymbol{\alpha}}(\boldsymbol{V}) = \Psi_{\boldsymbol{\alpha_\Theta}}(\boldsymbol{\Theta})\Psi_{\boldsymbol{\alpha_X}}(\boldsymbol{X})$, respectively. Following this decomposition, the PCE can be rearranged, leading to new coefficients which depend on a value for each of the statistical moments $\boldsymbol{\theta}$. Hence, for each combination of statistical moments, sampled from their corresponding uniform distributions, a Sobol' index can be quantified. Ultimately, the minimum and maximum Sobol' index for each stochastic input parameter can be found by an optimization approach, where the combination of possible statistical moments that leads to the lowest/highest Sobol' index is configured. Conclusively, for each stochastic parameter affected by aleatory uncertainty (precise or imprecise), an interval-ranged imprecise Sobol' index is quantified, for which the interval is determined through the random combinations of statistical moments from the input parameters affected by epistemic uncertainty. Details on the characterization of these imprecise Sobol' indices are found in Schöbi et al. [27].

2.6. Surrogate-assisted robust design optimization

The optimization objectives are minimizing the mean and minimizing the standard deviation of the aleatory uncertainty on the LCOX. Hence, by controlling the design variables (PV array capacity, battery capacity, ASHP capacity and thermal storage capacity), the optimizer aims to simultaneously minimize the effect of the irreducible aleatory uncertainty on the LCOX and minimize the average expected LCOX. The design that achieves the lowest LCOX standard deviation is identified as the robust design. This design is least-sensitive to its random environment and therefore ensures with the highest probability among the designs that the LCOX in reality situates near the LCOX mean. However, due to the additional epistemic uncertainty present on the stochastic input parameters characterized by a probability box, the real mean and real standard deviation of the LCOX are unknown, i.e. due to the uncertainty characterization in the form of probability boxes, the LCOX for each evaluated design is characterized by a probability box as well, with an upper bound and lower

bound on the mean and standard deviation. Therefore, the mean and standard deviation of the upper probability bound of the LCOX are selected as design objectives [33].

As the non-linear case is a multi-objective optimization problem, the Non-dominated Sorting Genetic Algorithm (NSGA-II) is selected as an optimization algorithm [68, 69]. The NSGA-II algorithm is implemented based on the Python library *deap* [70]. First, an initial population of design samples is created through Latin Hypercube sampling. For each design sample, an augmented PCE is constructed and the upper-bound mean and upper-bound standard deviation are quantified (subsection 2.5). The design samples are ranked based on their dominance in both objectives, leading to the next generation of design samples. This process is repeated until the computational budget is spent. In this work, the population size is fixed at 40 design samples, following a rule of thumb of 10 samples per design parameter [71]. The optimization algorithm is characterized by a crossover and mutation probability of 0.9 and 0.1, respectively.

3. Results and discussion

The results and discussion section presents and discusses the trade-off between minimizing the mean and standard deviation of the aleatory uncertainty on the LCOX. Then, the probability boxes for a set of optimized designs are analysed, to see how these results are affected by epistemic uncertainty. Finally, the Sobol' indices reveal the dominating stochastic parameters to the epistemic uncertainty on the LCOX. The results and discussion are subject to the following limitations of the approach: the stochastic model parameters are considered independent, i.e. the probability of each parameter is unaffected by the probability of the other parameters; the NSGA-II does not ensure mathematical optimality, i.e. the designs are optimized, but might not represent the optimal solution; due to limited data, the aleatory uncertainty of the stochastic parameters is represented by a Gaussian distribution. Nevertheless, the robust design optimization approach provides the design trends to reduce the LCOX stan-

dard deviation induced by uncertainty which is irreducible by data collection and it illustrates the advantages of a robust design as opposed to a design with an optimized LCOX mean. In addition, distinguishing between epistemic and aleatory uncertainty in the global sensitivity analysis identifies the main drivers of the epistemic uncertainty on the LCOX and thus highlights the parameters on which the knowledge should be improved, e.g. considering a specific energy demand profile as opposed to a generic one for an average household.

3.1. Robust design optimization on the aleatory uncertainty

In this section, the robust design optimization results are described for the previously introduced configurations: a PV-battery configuration with a gas boiler that covers the entire heat demand; a PV-battery-ASHP configuration, where the power to run the ASHP comes from the excess PV electricity and grid electricity; a PV-battery ASHP configuration where the excess of PV electricity and stored electricity in the bank of batteries are used to run the ASHP, before the grid electricity is called upon.

3.1.1. PV-battery-gas boiler

For the RDO of a PV-battery-gas boiler system, a trade-off exists between minimizing the LCOX mean and minimizing the LCOX standard deviation (Figure 6, top). Hence, the optimizer is unable to generate a single PV-battery-gas boiler design that simultaneously achieves the minimized LCOX mean and LCOX standard deviation. The Pareto front illustrates that the optimized mean design (i.e. the design that achieves the lowest upper-bound LCOX mean) achieves an LCOX mean of 623 €/MWh and an LCOX standard deviation of 109.8 €/MWh. Instead, the robust design (i.e. the design that achieves the lowest upper-bound LCOX standard deviation) achieves an LCOX mean of 730 €/MWh and an LCOX standard deviation of 106.7 €/MWh. These extreme designs on the Pareto front consist of a 1.8 kW_p PV array and of an 8.0 kW_p PV array - 7.9 kWh bank of batteries, respectively. Despite the trade-off, the difference in LCOX standard deviation between the optimized mean design and the

robust design is limited (3.1 €/MWh or 2.8 %). Hence, the robust alternative to the optimized mean design is only slightly less sensitive to its random environment. However, an intermediate design on the Pareto front, achieving an LCOX mean of 636 €/MWh and an LCOX standard deviation of 107.7 €/MWh (grey dot in Figure 6), reduces the LCOX standard deviation by 2 % when compared to the optimized mean design, at the expense of a 2 % increase in LCOX mean. Therefore, this intermediate design, consisting of a 2.2 kW_p PV array and a 3.2 kWh bank of batteries, provides a viable robust alternative to the optimized mean design.

The reason why the robust design is only slightly more robust than the optimized mean design comes from the complete dependency on the natural gas to comply with the heat demand (Figure 6, bottom). Indeed, despite the effect of epistemic uncertainty on the imprecise Sobol' indices (i.e. the epistemic uncertainty is the driver of the range of the imprecise Sobol' index), it can be concluded that the aleatory uncertainty of the natural gas price (i.e. the aleatory uncertainty is the driver of the mean of the imprecise Sobol' index) dominates the characterization of the true-but-unknown LCOX standard deviation. To illustrate, the true-but-unknown Sobol' index for the optimized mean design situates between 0.8 and 0.95, while the true-but-unknown Sobol' indices for the electricity price and electricity demand situate between 0.05 and 0.16 and between 0.00 and 0.04, respectively. Conclusively, considering a PV array with a bank of batteries is a viable robust alternative for the optimized mean design, which consists of solely a PV array. Nevertheless, due to the dominance of the gas price aleatory uncertainty on the LCOX standard deviation, the gain in robustness for the robust alternative is limited.

3.1.2. PV-battery-ASHP

By considering an electrically-driven ASHP to cover the heat demand, the gas dependency is eliminated and the generated electricity by the PV array is employed to comply with both the electricity demand and heat demand.

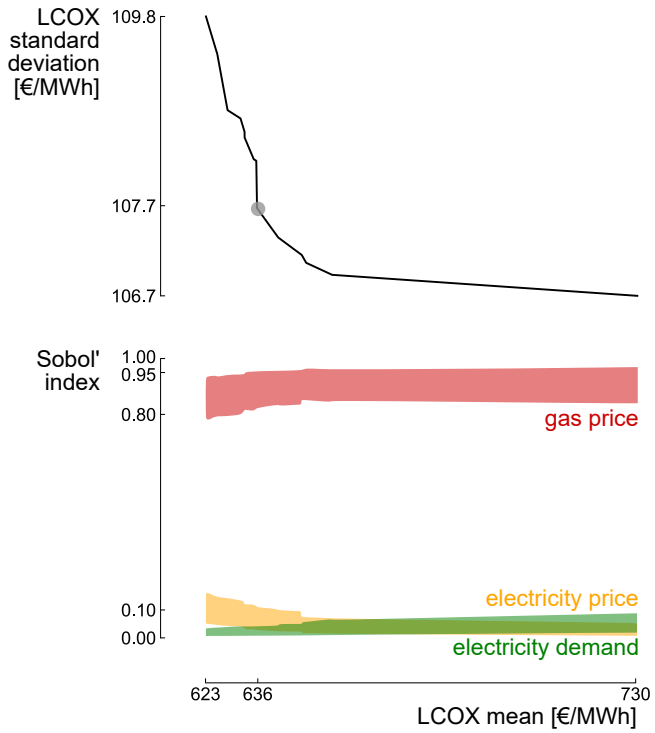

Figure 6: The Pareto front between minimizing the LCOX mean and minimizing the LCOX standard deviation illustrates that the gain in robustness is limited when shifting between optimized mean and robust design (top figure). The Sobol' indices explain this limited gain in robustness by illustrating that the aleatory uncertainty on the gas price (bottom figure), which is irreducible by designing the PV array and battery capacity, is the main driver of the true-but-unknown LCOX standard deviation.

Pareto front. When comparing the achieved Pareto fronts for the PV-battery-ASHP configurations with the Pareto front for the PV-battery-gas boiler configuration, the optimized LCOX standard deviation on the Pareto front is significantly lower for the PV-battery-ASHP optimized designs than for the PV-battery-gas boiler optimized designs (Figure 7). To illustrate, an intermediate optimized design (i.e. situated between the extreme designs on the Pareto front, indicated with a grey dot in Figure 7) for a PV-battery-ASHP system with a battery support power management strategy achieves an upper-bound LCOX standard deviation of 70.0 €/MWh, which reduces the standard deviation by 36 % as opposed to the PV-battery-gas boiler design with an upper-bound LCOX

standard deviation of 109.8 €/MWh. However, the optimized LCOX mean values for the PV-battery-ASHP designs are higher than for the PV-battery-gas boiler designs (e.g. 39 % higher between the two previously compared designs). Similar conclusions on the fact that an ASHP with thermal storage has higher deterministic costs than a conventional gas boiler system were also presented by Renaldi et al. [72]. When comparing the optimized designs from both power management strategies in the PV-battery-ASHP configuration, the corresponding Pareto fronts illustrate that the LCOX standard deviation can be further reduced when the strategy with battery support for the ASHP is considered as opposed to when the strategy without battery support for the ASHP is considered. Conclusively, a PV-battery-ASHP configuration can provide a cost-competitive, robust alternative to a PV-battery-gas boiler configuration.

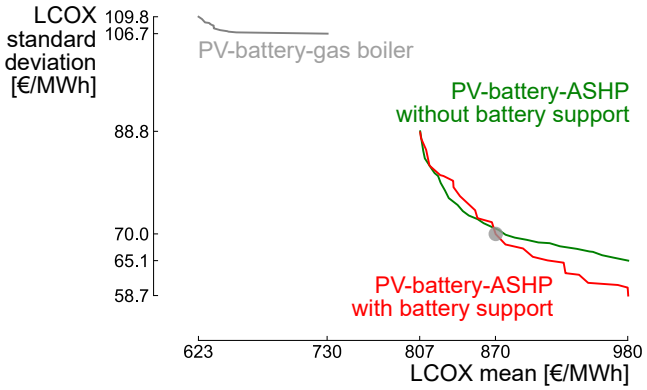

Figure 7: The Pareto fronts for the PV-battery-ASHP configurations, which connect the LCOX mean and LCOX standard deviation for the optimized designs of each configuration, illustrate that the optimized PV-battery-ASHP designs achieve a higher LCOX mean than the optimized PV-battery-gas boiler designs. However, the optimized PV-battery-ASHP design achieve a significantly lower LCOX standard deviation.

Component capacities. To clarify the Pareto fronts, the PV self-consumption rate (i.e. the portion of the generated PV electricity that is consumed by the electricity demand), annual grid electricity consumed and the component capacities for the optimized PV-battery-ASHP designs are presented in function of the LCOX mean in Figure 8. For both sets of optimized designs (i.e. the

PV-battery-ASHP with battery support and PV-battery-ASHP without battery support sets of optimized designs which resulted in the Pareto fronts in Figure 7), the PV array capacity evolves similarly from the optimized mean design to the robust design (i.e. the designs which achieve an upper-bound LCOX mean of 807 €/MWh and 980 €/MWh, respectively). For the optimized LCOX mean design in both power management strategies, no battery storage is considered. Hence, the difference in power management strategy has no effect on the LCOX, as no battery support to run the ASHP is available. However, the trend towards the robust designs (i.e. with an LCOX mean of 980 €/MWh) illustrate that the PV-battery-ASHP configuration with battery support considers a higher capacity for the bank of batteries than the PV-battery-ASHP configuration without battery support. To illustrate, a design for the strategy without battery support, which achieves an LCOX mean of 870 €/MWh, consists of a 3.3 kWh bank of batteries, while the design for the strategy with battery support and with the same LCOX mean (870 €/MWh) consists of a 7.5 kWh bank of batteries (the characteristics of these designs are indicated by grey dots in Figure 8). Evidently, the latter achieves a lower annual grid electricity consumption (5.3 MWh) than the former (5.5 MWh). Nevertheless, the annual grid electricity consumption remains significant, as the battery capacity is limited and sized for daily storage. Moreover, the evolution of the battery capacity closely relates to the PV self-consumption. As a larger share of PV excess electricity can be stored in the bank of batteries for the designs considering battery support, this strategy achieves a higher PV self-consumption than the strategy without battery support. To illustrate for the previously compared designs, the PV self-consumption is 59 % and 40 %, respectively. In both strategies, the ASHP capacity of the optimized designs ranges between 5.8 kW_{th} and 8.3 kW_{th}, while the thermal storage ranges between 256 l and 399 l. The ASHP and thermal storage capacities are similar to the ones presented in the deterministic design optimization of an ASHP with thermal storage in the United Kingdom under different electricity tariffs (8.5 kW_{th} and 300 l) [72]. The fact that thermal storage is considered in every optimized design indicates that ther-

mal storage is beneficial for improving the LCOX mean and LCOX robustness over the system lifetime. Similarly, Renaldi et al. [72] indicated that combining thermal energy storage with ASHP results in a smaller cost as opposed to not considering thermal storage. Nevertheless, this relatively small thermal energy storage capacity is only suitable for daily thermal energy storage, as the significant heat loss limits the application of seasonal storage in its current form.

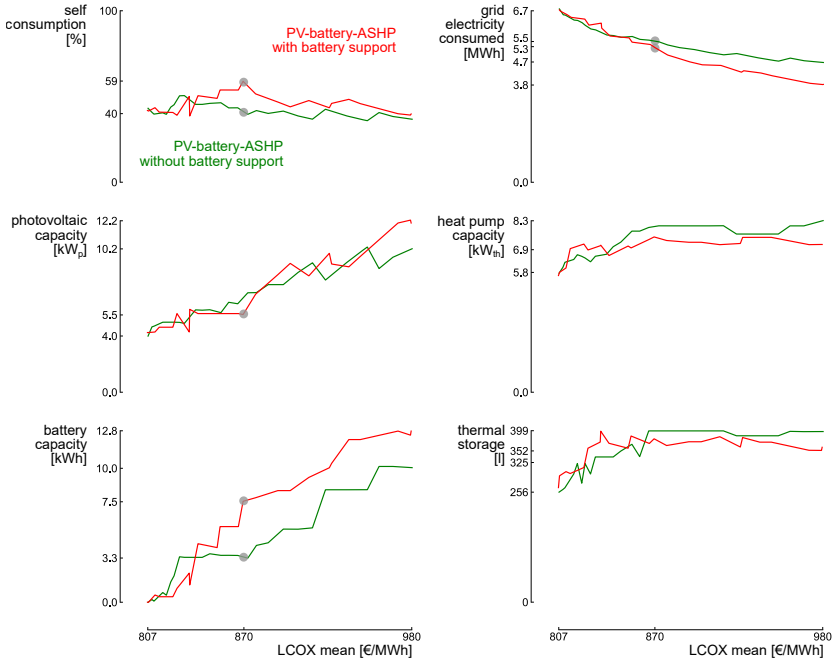

Figure 8: The PV self-consumption, annual grid electricity consumption and system capacities in function of the LCOX mean for the optimized designs for the two power management strategies of the PV-battery-ASHP configurations. In most optimized designs under the strategy with battery support, a significantly larger battery is considered, which results in a lower annual grid electricity consumption and a higher PV self-consumption than for the optimized designs under the strategy without battery support.

Imprecise Sobol' indices. To understand the evolution of the LCOX standard deviation on the Pareto fronts for the two power management strategies, the imprecise Sobol' indices are quantified for the optimized designs (Figure 9). Clearly, the uncertainty on the future grid electricity price dominates the LCOX

Table 1: The characteristics of the three representative designs for the photvoltaic-battery-ASHP management strategies: an optimized mean design (lowest upper-bound LCOX mean), an intermediate design and a robust design (lowest upper-bound LCOX standard deviation).

	N_{PV} kW_p	N_{bat} kWh	N_{hp} kW_th	$N_{\text{thermal storage}}$ l	μ_{LCOX} €/MWh	σ_{LCOX} €/MWh
without battery support						
optimized mean	4.0		5.8	256	[396,807]	[57.6,88.8]
intermediate	5.8	3.3	8.3	399	[438,872]	[47.1,70.2]
robust	10.2	10.0	8.3	397	[473,980]	[34.5,65.1]
with battery support						
optimized mean	4.2		5.6	266	[397,807]	[54.6,88.8]
intermediate	5.5	7.5	6.9	325	[435,870]	[41.0,70.0]
robust	12.2	12.8	7.2	352	[465,980]	[27.7,58.7]

standard deviation. This conclusion can be made despite the overall epistemic uncertainty on the stochastic parameters, which induces the range on the imprecise Sobol' indices, as the imprecise Sobol' indices barely overlap. However, for the robust design of the strategy with battery support, the Sobol' index range for the electricity price and electricity demand clearly overlap. This indicates that for this specific design, it remains inconclusive which parameter is the most dominant driver of the true-but-unknown LCOX standard deviation, due to the overall epistemic uncertainty on the stochastic parameters.

The reducing trend in the imprecise Sobol' index of the electricity price implies a decreasing dependency on the grid electricity to comply with the energy demand. This reducing trend is larger under the battery support strategy, as the battery storage reduces the grid electricity consumption of the ASHP by covering part of the ASHP demand when the solar irradiance is insufficient (e.g. at night). The increasing trend on the importance of the aleatory uncertainty of the electricity demand corresponds to an increased photovoltaic array and battery capacity, for which its economic effectiveness depends on the match with the electricity demand.

Finally, the effect of the heat demand aleatory uncertainty on the LCOX

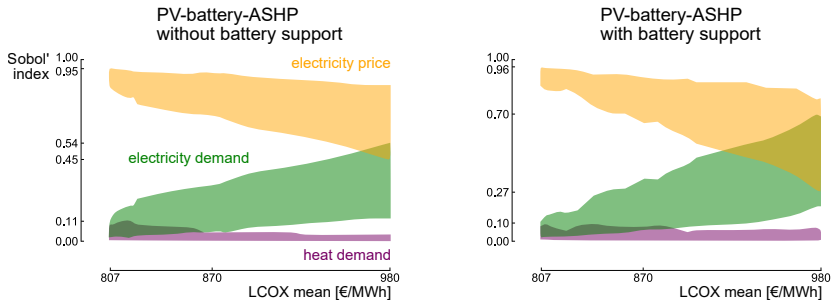

Figure 9: The evolution of the Sobol' indices for the stochastic parameters on the set of optimized designs indicate that the uncertainty on the future electricity price is the dominant uncertainty for the LCOX for most optimized designs. For the robust design, it remains inconclusive if the aleatory uncertainty on the electricity price or on the electricity demand is the main driver, due to epistemic uncertainty.

is small. This is mainly due to the reduced weight of the heat demand by the Carnot coefficient in an exergy environment (Equation 25).

3.2. Probability box characterization for optimized designs

In the previous section, the designs are configured to minimize the effect of aleatory uncertainty on the expected LCOX, while maintaining an optimized LCOX mean. To study the effect of the epistemic uncertainty on the LCOX over the system lifetime, the LCOX p-boxes for a set of representative designs are analysed (i.e. optimized mean design, intermediate design and robust design, Table 1). The effect of the epistemic uncertainty on these three representing designs is comparable between both strategies (i.e. range on the statistical moments in Table 1 and width of the p-box in Figure 10). When comparing between the three representative designs, the robust design is clearly more affected by epistemic uncertainty. Nevertheless, given the overall epistemic uncertainty, the p-boxes of the three representing designs for both strategies overlap. Therefore, at this step, it remains inconclusive which design achieves the most favourable true-but-unknown CDF.

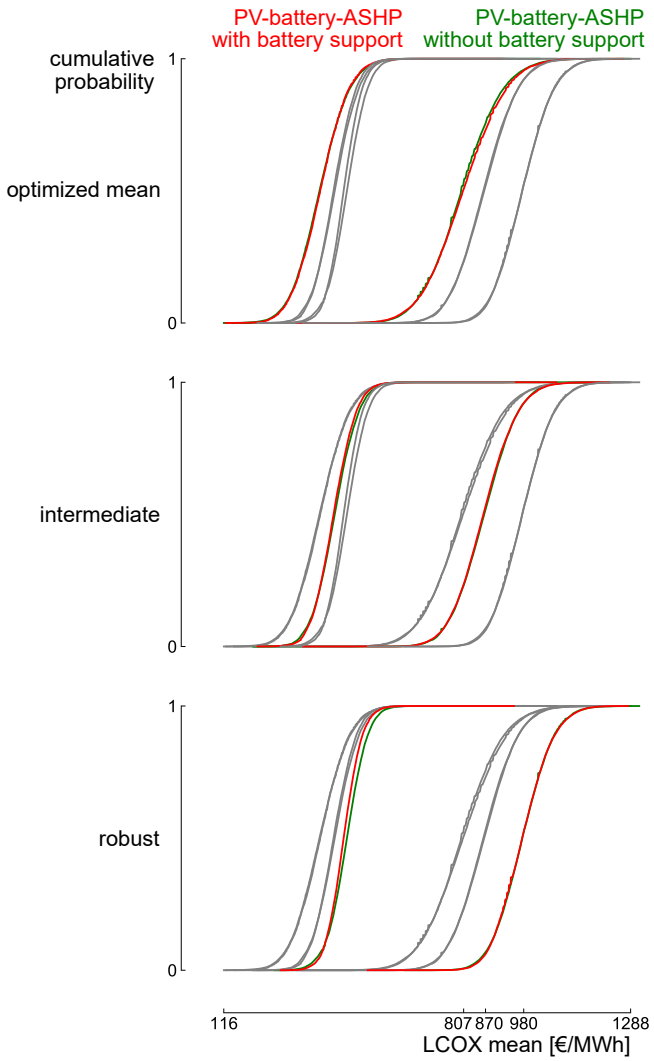

Figure 10: The probability boxes for the optimized mean design, intermediate design and robust design for both PV-battery-heap pump configurations indicate that the difference in the effect of the epistemic uncertainty is negligible between configurations.

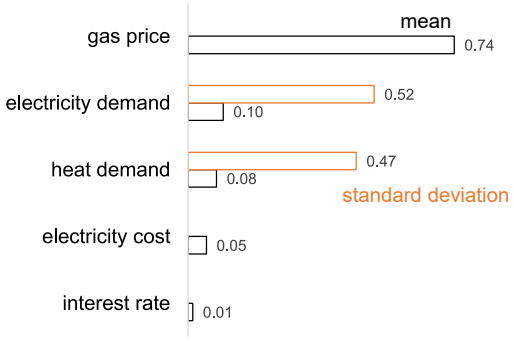

Figure 11: Top-5 total order Sobol' indices related to the epistemic uncertainty on the LCOX of the optimized mean PV-battery-gas boiler design.

3.3. Global sensitivity analysis on the epistemic uncertainty

To determine the true-but-unknown CDF of the optimized designs, the epistemic uncertainty must be reduced. To characterize what contributes to the epistemic uncertainty on the LCOX of these designs, we performed a global sensitivity analysis on the epistemic uncertainty of the p-boxes. As the epistemic uncertainty affects both the mean and standard deviation (Table 1), two sets of Sobol' indices are generated for each p-box.

For the optimized LCOX mean design of the PV-battery-gas boiler configuration, the epistemic uncertainty on the LCOX mean (and thus width of the p-box) is dominated by the epistemic uncertainty on the gas price (Figure 11). Hence, to determine the expected LCOX performance of this design, the main action is to determine the gas supplier and the corresponding contract. The uncertainty on the occupant behaviour in electricity demand and heat demand contribute equally (i.e. a Sobol' index of 52 % and 47 %, respectively) to the epistemic uncertainty on the LCOX standard deviation. Therefore, adopting heat demand and electricity demand profiles for a specific household with information on the occupant behaviour drastically improves the knowledge on the LCOX standard deviation and thus on the robust performance of the specific design.

For the optimized LCOX mean designs for both power management strate-

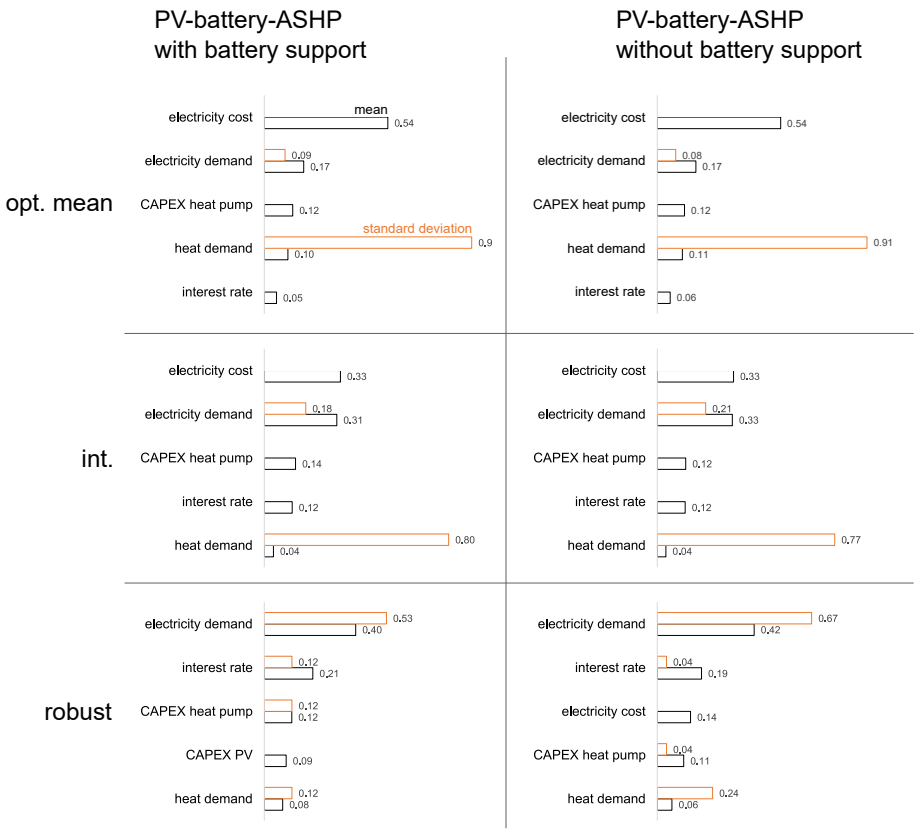

Figure 12: Top-5 total order Sobol' indices related to the epistemic uncertainty on the LCOX for the optimized mean (opt. mean), intermediate (interm.) and robust PV-battery-ASHP designs.

gies of the PV-battery-ASHP configuration (Table 1), the epistemic uncertainty on the electricity price dominates the uncertainty on the mean LCOX (Figure 12, *opt. mean*). For the epistemic uncertainty on the standard deviation, the dominating contribution comes from the uncertainty on the occupant behaviour regarding the heat demand. As both designs do not include a bank of batteries, there is no difference due to the power management strategy and therefore the difference between the top-5 Sobol' indices is minimal.

For the intermediate designs, the epistemic uncertainties on the electricity price and electricity demand are the most significant contributors to the uncertainty on the LCOX mean (Figure 12, *int.*). Also, the epistemic uncertainty on

the CAPEX for the heat pump gains significant importance. Hence, specifying the specific heat pump technology and its corresponding market condition becomes a significant action to reduce the epistemic uncertainty on the mean LCOX for these intermediate designs. For the uncertainty on the LCOX standard deviation, the epistemic uncertainty on the heat demand is again the main driver. Finally, for the robust designs, the epistemic uncertainty on the electricity demand dominates both the epistemic uncertainty on the LCOX mean and LCOX standard deviation (Figure 12, *robust*). Hence, gaining knowledge on the occupant behaviour related to the electricity demand is the most effective measure to clarify both performance and robustness of these designs.

Conclusively, considering a specific electricity demand and heat demand profile for a specific household, and thus reducing the epistemic uncertainty of using generic profiles, are the main actions to determine the true-but-unknown LCOX standard deviation for these representative designs. Reducing the epistemic uncertainty related to the electricity demand is also the main action to clarify the true-but-unknown mean LCOX for the intermediate PV-battery-ASHP designs and the robust designs, while gaining information on the grid electricity contract and supplier is significant for both optimized LCOX mean designs. Finally, the epistemic uncertainty induced by considering generic ASHP technology is significant, while the effect of considering generic technology models for the other components is minor.

4. Conclusion

Sector coupling of heating and electricity improves the decarbonization of the heating sector. In this framework, Air-Source Heat Pumps (ASHP) provide an adequate approach to realise this coupling. For a photovoltaic-battery-heat pump configuration, a robust design optimization on the aleatory uncertainty of the Levelized Cost Of eXergy (LCOX) illustrates that the robustness towards LCOX aleatory uncertainty can be improved by 36 % when compared to a photovoltaic-battery-gas boiler configuration, at the expense of a 39 % increase

in LCOX mean. The robustness is optimized when both excess PV electricity and stored electricity in the battery are considered to run the ASHP, as opposed to using the battery electricity only to cover the household electricity demand. Additionally, in these optimized photovoltaic-battery-heat pump designs, thermal energy storage is consequently considered by the optimizer for short-term energy storage (i.e. days), which indicates that thermal storage is beneficial for improving the LCOX mean and LCOX robustness over the system lifetime. Conclusively, PV-battery-ASHP configurations provide a cost-competitive, robust alternative to PV-battery-gas boiler configurations.

In between the optimized set of PV-battery-ASHP designs, it remains inconclusive which design results in optimized expected performance and which design is the most robust, due to the overall epistemic uncertainty present on the LCOX. To reduce the epistemic uncertainty effectively on the LCOX mean (and thus on the expected performance), gaining information on the grid electricity contract is the main action for the optimized LCOX mean designs. This action proves also significant for an intermediate design (i.e. a design which considers a trade-off between minimized LCOX mean and LCOX standard deviation), in addition to considering a specific electricity demand profile for a household. For the epistemic uncertainty on the LCOX standard deviation, the uncertainties on the occupant behaviour regarding electricity demand and heat demand are the main drivers. Therefore, specific heat demand and electricity demand profiles enable to characterize the true-but-unknown robustness toward variability in the LCOX due to aleatory uncertainty. Finally, the epistemic uncertainty induced by considering generic technology models as opposed to a specific type proves to be negligible in the epistemic uncertainty on the statistical moments of the LCOX, except for the ASHP.

In future work, different electricity tariffs and corresponding power management strategies will be evaluated. To illustrate, with a variable electricity tariff, the strategy can take advantage of low grid electricity prices to run the heat pump, charge the battery or charge the thermal storage with grid electricity. Additionally, the implementation of lithium-ion batteries will be considered. De-

spite the higher cost and higher uncertainty on the cost, the technology promises higher power and energy density. Finally, an electric vehicle will be added to the household demand, which will improve the self-consumption of the photovoltaic array.

5. Acknowledgements

The first author acknowledges the support of Fonds de la Recherche Scientifique - FNRS [35484777 FRIA-B2].

Appendix A. Data

Table A.2: Parameters affected by aleatory and epistemic uncertainty and thus characterized by a parametric probability-box. The true-but-unknown mean and standard deviation characterize the aleatory uncertainty. The range on the mean is induced by epistemic uncertainty.

parameter	mean	standard deviation	unit	Ref.
grid electricity price	[252,370]	68.9	€/MWh	[58, 60]
gas price	[50,86]	22.6	€/MWh	[59, 60]
electricity demand	[2.53,3.43]	0.22	MWh/year	[62, 63]
heat demand	[11.1,15.1]	1.1	MWh/year	[61, 63]

Table A.3: Parameters affected by aleatory uncertainties

parameter	mean	standard deviation	unit	Ref.
annual solar irradiance	1174	92	kWh/m^2	[73]
average ambient temperature	10.3	0.4	°C	[73]
inflation rate	1	3	%	[65]

Table A.4: Parameters affected by epistemic uncertainty

parameter	min	max	unit	Ref.
CAPEX_{PV}	350	600	€/kW_{p}	[1]
OPEX_{PV}	16	19	€/kW_{p}/year	[74]
$\text{CAPEX}_{\text{bat}}$	102	354	€/kWh	[43]
OPEX_{bat}	15	28	€/kWh	[43, 45]
$R_{\text{c,bat}}$	61	141	€/kWh/year	[43, 45]
n_{bat}	500	2000	cycles	[43]
self $\text{discharge}_{\text{bat}}$	0.1	0.3	%/day	[45]
CAPEX_{hp}	600	1100	€/kW_{th}	[75, 76]
OPEX_{hp}	3.7	15	€/kW_{th}/year	[75, 76]
$\text{CAPEX}_{\text{thermal storage}}$	2.8	5.4	€/l	[75, 77]
$\text{CAPEX}_{\text{gas boiler}}$	110	200	€/kW_{th}	[75, 78]
$\text{OPEX}_{\text{gas boiler}}$	2.5	5	% of $\text{CAPEX}_{\text{gas boiler}}$	[75, 78]
$\text{CAPEX}_{\text{DCDC}}$	40	160	€/kW	[79, 80]
$\text{OPEX}_{\text{DCDC}}$	1	5	% of $\text{CAPEX}_{\text{DCDC}}$	[81, 82]
$\text{CAPEX}_{\text{DCAC}}$	50	200	€/kW	[79]
$\text{OPEX}_{\text{DCAC}}$	1	5	% of $\text{CAPEX}_{\text{DCAC}}$	[81, 82]
interest rate	4	8	%	[83–85]

References

[1] International Energy Agency, Renewables 2019: Analysis and forecast to 2024, Tech. rep., International Energy Agency (2019).

[2] A. Gravelsins, I. Pakere, A. Tukulis, D. Blumberga, Solar power in district heating. P2H flexibility concept, Energy 181 (2019) 1023–1035.

[3] REN21, Renewables 2020 global status report, Tech. rep., REN21 (2020).

[4] H. Lund, Renewable heating strategies and their consequences for storage and grid infrastructures comparing a smart grid to a smart energy systems approach, Energy 151 (2018) 94–102.

[5] S. Murugan, B. Horák, Tri and polygeneration systems-A review, Renewable and Sustainable Energy Reviews 60 (2016) 1032–1051.

[6] G. Kyriakarakos, A. I. Dounis, S. Rozakis, K. G. Arvanitis, G. Papadakis, Polygeneration microgrids: a viable solution in remote areas for supplying power, potable water and hydrogen as transportation fuel, Applied Energy 88 (12) (2011) 4517–4526.

[7] M. A. V. Rad, R. Ghasempour, P. Rahdan, S. Mousavi, M. Arastounia, Techno-economic analysis of a hybrid power system based on the cost-effective hydrogen production method for rural electrification, a case study in Iran, Energy 190 (2020) 116421.

[8] R. Luthander, J. Widén, D. Nilsson, J. Palm, Photovoltaic self-consumption in buildings: A review, Applied energy 142 (2015) 80–94.

[9] H. Lund, P. A. Østergaard, D. Connolly, B. V. Mathiesen, Smart energy and smart energy systems, Energy 137 (2017) 556–565.

[10] H. Lund, P. A. Østergaard, M. Chang, S. Werner, S. Svendsen, P. Sorknæs, J. E. Thorsen, F. Hvelplund, B. O. G. Mortensen, B. V. Mathiesen, et al., The status of 4th generation district heating: Research and results, Energy 164 (2018) 147–159.

[11] H. Wolisz, T. Schütz, T. Blanke, M. Hagenkamp, M. Kohrn, M. Wesseling, D. Müller, Cost optimal sizing of smart buildings' energy system components considering changing end-consumer electricity markets, Energy 137 (2017) 715–728.

[12] A.-L. Klingler, The effect of electric vehicles and heat pumps on the market potential of PV+battery systems, Energy 161 (2018) 1064–1073.

[13] G. Angenendt, S. Zurmühlen, J. Figgener, K.-P. Kairies, D. U. Sauer, Providing frequency control reserve with photovoltaic battery energy storage systems and power-to-heat coupling, Energy 194 (2020) 116923.

[14] G. Angenendt, S. Zurmühlen, F. Rücker, H. Axelsen, D. U. Sauer, Optimization and operation of integrated homes with photovoltaic battery energy storage systems and power-to-heat coupling, Energy Conversion and Management: X 1 (2019) 100005.

[15] G. Mavromatidis, K. Orehounig, J. Carmeliet, A review of uncertainty characterisation approaches for the optimal design of distributed energy systems, Renewable and Sustainable Energy Reviews 88 (2018) 258–277.

[16] Y. Yin, T. Liu, L. Wu, C. He, Y. Liu, Frequency-constrained multi-source power system scheduling against N-1 contingency and renewable uncertainty, Energy (2020) 119296.

[17] Y. Zhang, Y. Liu, S. Shu, F. Zheng, Z. Huang, A data-driven distributionally robust optimization model for multi-energy coupled system considering the temporal-spatial correlation and distribution uncertainty of renewable energy sources, Energy 216 (2020) 119171.

[18] R. Koubaa, S. Bacha, M. Smaoui, et al., Robust optimization based energy management of a fuel cell/ultra-capacitor hybrid electric vehicle under uncertainty, Energy (2020) 117530.

[19] T. Wakui, K. Sawada, R. Yokoyama, H. Aki, Predictive management for energy supply networks using photovoltaics, heat pumps, and battery by two-stage stochastic programming and rule-based control, Energy 179 (2019) 1302–1319.

[20] X. Yang, Y. Liu, Y. Zhang, Z. Yue, Hybrid reliability analysis with both random and probability-box variables, Acta Mechanica 226 (5) (2015) 1341–1357.

[21] T. Augustin, F. P. Coolen, G. De Cooman, M. C. Troffaes, Introduction to imprecise probabilities, John Wiley & Sons, 2014.

[22] A. Der Kiureghian, O. Ditlevsen, Aleatory or epistemic? Does it matter?, Structural safety 31 (2) (2009) 105–112.

[23] S. Moret, V. C. Gironès, M. Bierlaire, F. Maréchal, Characterization of input uncertainties in strategic energy planning models, Applied energy 202 (2017) 597–617.

[24] A. Younesi, H. Shayeghi, A. Safari, P. Siano, Assessing the resilience of multi microgrid based widespread power systems against natural disasters using Monte Carlo Simulation, Energy 207 (2020) 118220.

[25] Z. Deng, X. Hu, X. Lin, Y. Che, L. Xu, W. Guo, Data-driven state of charge estimation for lithium-ion battery packs based on Gaussian process regression, Energy 205 (2020) 118000.

[26] L. Daróczy, G. Janiga, D. Thévenin, Analysis of the performance of a H-Darrieus rotor under uncertainty using Polynomial Chaos Expansion, Energy 113 (2016) 399–412.

[27] R. Schöbi, B. Sudret, Global sensitivity analysis in the context of imprecise probabilities (p-boxes) using sparse polynomial chaos expansions, Reliability Engineering & System Safety 187 (2019) 129–141.

[28] D. Coppitters, W. De Paepe, F. Contino, Surrogate-assisted robust design optimization and global sensitivity analysis of a directly coupled photovoltaic-electrolyzer system under techno-economic uncertainty, Applied Energy 248 (2019) 310–320.

[29] I. Doltsinis, Z. Kang, Robust design of structures using optimization methods, Computer methods in applied mechanics and engineering 193 (23-26) (2004) 2221–2237.

[30] W. De Paepe, D. Coppitters, S. Abraham, P. Tsirikoglou, G. Ghorbaniasl, F. Contino, Robust Operational Optimization of a Typical micro Gas Turbine, Energy Procedia 158 (2019) 5795–5803.

[31] D. Coppitters, W. De Paepe, F. Contino, Robust design optimization and stochastic performance analysis of a grid-connected photovoltaic system with battery storage and hydrogen storage, Energy 213 (2020) 118798.

[32] Z. Hu, X. Du, N. S. Kolekar, A. Banerjee, Robust design with imprecise random variables and its application in hydrokinetic turbine optimization, Engineering Optimization 46 (3) (2014) 393–419.

[33] X. Xie, R. Schenkendorf, Robust process design in pharmaceutical manufacturing under batch-to-batch variation, Processes 7 (8) (2019) 509.

[34] B. M. Radhakrishnan, D. Srinivasan, A multi-agent based distributed energy management scheme for smart grid applications, Energy 103 (2016) 192–204.

[35] M. Barma, R. Saidur, S. Rahman, A. Allouhi, B. Akash, S. M. Sait, A review on boilers energy use, energy savings, and emissions reductions, Renewable and Sustainable Energy Reviews 79 (2017) 970–983.

[36] M. Liu, S. Wang, Y. Zhao, H. Tang, J. Yan, Heat-power decoupling technologies for coal-fired CHP plants: Operation flexibility and thermodynamic performance, Energy 188 (2019) 116074.

[37] D. Fischer, H. Madani, On heat pumps in smart grids: A review, Renewable and Sustainable Energy Reviews 70 (2017) 342–357.

[38] W. F. Holmgren, C. W. Hansen, M. A. Mikofski, pvlib python: a python package for modeling solar energy systems, The Journal of Open Source Software 3 (2018) 884.

[39] T. Gurupira, A. Rix, Pv simulation software comparisons: Pvsyst, nrel sam and pvlib, in: Conf.: SAUPEC, 2017.

[40] W. De Soto, S. A. Klein, W. A. Beckman, Improvement and validation of a model for photovoltaic array performance, Solar Energy 80 (1) (2006) 78–88.

[41] Sunpower, X-Series residential solar panels: supplementary technical specifications.

[42] G. de Oliveira e Silva, P. Hendrick, Lead–acid batteries coupled with photovoltaics for increased electricity self-sufficiency in households, Applied Energy 178 (2016) 856–867.

[43] B. Battke, T. S. Schmidt, D. Grosspietsch, V. H. Hoffmann, A review and probabilistic model of lifecycle costs of stationary batteries in multiple applications, Renewable and Sustainable Energy Reviews 25 (2013) 240–250.

[44] S. Blaifi, S. Moulahoum, I. Colak, W. Merrouche, An enhanced dynamic model of battery using genetic algorithm suitable for photovoltaic applications, Applied Energy 169 (2016) 888–898.

[45] B. Zakeri, S. Syri, Electrical energy storage systems: A comparative life cycle cost analysis, Renewable and sustainable energy reviews 42 (2015) 569–596.

[46] G. Díaz, J. Gómez-Aleixandre, J. Coto, O. Conejero, Maximum income resulting from energy arbitrage by battery systems subject to cycle aging and price uncertainty from a dynamic programming perspective, Energy 156 (2018) 647–660.

[47] C. Phurailatpam, B. S. Rajpurohit, L. Wang, Planning and optimization of autonomous DC microgrids for rural and urban applications in India, Renewable and Sustainable Energy Reviews 82 (2018) 194–204.

[48] C. P. Underwood, M. Royapoor, B. Sturm, Parametric modelling of domestic air-source heat pumps, Energy and Buildings 139.

[49] G. A. Rampinelli, A. Krenzinger, F. Chenlo Romero, Mathematical models for efficiency of inverters used in grid connected photovoltaic systems, Renewable and Sustainable Energy Reviews 34 (2014) 578–587.

[50] M. Taghvaee, M. Radzi, S. Moosavain, H. Hizam, M. H. Marhaban, A current and future study on non-isolated DC–DC converters for photovoltaic applications, Renewable and sustainable energy reviews 17 (2013) 216–227.

[51] S. Wilcox, W. Marion, Users manual for TMY3 data sets, Tech. rep., National Renewable Energy Laboratory Golden, CO (2008).

[52] Open Energy Information, Commercial and Residential Hourly Load Profiles for all TMY3 Locations in the United States, Available online: http://en.openei.org/datasets/dataset/commercial-and-residential-hourly-load-profiles-for-all-tmy3-\locations-in-the-united-states. Accessed: 16th June 2020.

[53] M. Montero Carrero, I. R. Sánchez, W. D. Paepe, A. Parente, F. Contino, Is There a Future for Small-Scale Cogeneration in Europe ? Economic and Policy Analysis of the Internal Humid Air Turbine Cycles, Energies 12 (3) (2019) 1–27.

[54] R. Hendron, C. Engebrecht, Building america house simulation protocols, Tech. rep., National Renewable Energy Laboratory (2010).

[55] R. Sangi, P. M. Martín, D. Müller, Thermoeconomic analysis of a building heating system, Energy 111 (2016) 351–363.

[56] VREG - Flemish Energy Regulator of the electricity and gas market, Marktrapport 2019, Tech. rep., Vlaamse Regulator van de Elektriciteits- en Gasmarkt, Available online: https://www.vreg.be/sites/default/files/document/rapp-2020-10.pdf. Accessed: 28th January 2021 (2020).

[57] M. Di Somma, B. Yan, N. Bianco, G. Graditi, P. Luh, L. Mongibello, V. Naso, Multi-objective design optimization of distributed energy systems through cost and exergy assessments, Applied Energy 204 (2017) 1299–1316.

[58] Elia, Electricity scenarios for Belgium towards 2050: Elia's quantified study on the energy transition in 2030 and 2040, Tech. rep., Elia (2017).

[59] I. Duić, N. Štefanić, Z. Lulić, G. Krajačić, T. Pukšec, T. Novosel, EU28 fuel prices for 2015, 2030 and 2050. Deliverable 6.1: Future fuel price review (2017).

[60] PricewaterhouseCoopers, Vergelijking van de elektriciteitsen aardgastarieven, Tech. rep., Vlaamse Regulator van de Elektriciteits- en Gasmarkt (2019).

[61] S. Gendebien, E. Georges, S. Bertagnolio, V. Lemort, Methodology to characterize a residential building stock using a bottom-up approach: a case study applied to Belgium, International Journal of Sustainable Energy Planning and Management 4 (2014) 71–88.

[62] Climact, Electrical energy savings scenarios for Belgium, Tech. rep., Climact (2012).

[63] W. Tian, Y. Heo, P. De Wilde, Z. Li, D. Yan, C. S. Park, X. Feng, G. Augenbroe, A review of uncertainty analysis in building energy assessment, Renewable and Sustainable Energy Reviews 93 (2018) 285–301.

[64] D. S. Ryberg, J. Freeman, N. Blair, Quantifying interannual variability for photovoltaic systems in PVWatts, Tech. rep., National Renewable Energy Lab.(NREL), Golden, CO (United States) (2015).

[65] Triami Media BV, Historic inflation Belgium - CPI inflation, Available online: `inflation.eu/inflation-rates/belgium/historic-inflation/cpi-inflation-belgium.aspx`. Accessed: 1st August 2020 (2019).

[66] S. Abraham, M. Raisee, G. Ghorbaniasl, F. Contino, C. Lacor, A robust and efficient stepwise regression method for building sparse polynomial chaos expansions, Journal of Computational Physics 332 (2017) 461–474.

[67] B. Sudret, Polynomial chaos expansions and stochastic finite-element methods, Risk and Reliability in Geotechnical Engineering Chap. 6 (2003) (2014) 265–300.

[68] K. Verleysen, D. Coppitters, A. Parente, W. De Paepe, F. Contino, How can power-to-ammonia be robust? Optimization of an ammonia synthesis plant powered by a wind turbine considering operational uncertainties, Fuel 266 (2020) 117049.

[69] S. Giorgetti, D. Coppitters, F. Contino, W. D. Paepe, L. Bricteux, G. Aversano, A. Parente, Surrogate-Assisted Modeling and Robust Optimization of a Micro Gas Turbine Plant With Carbon Capture, Journal of Engineering for Gas Turbines and Power 142 (1).

[70] F.-A. Fortin, F.-M. De Rainville, M.-A. G. Gardner, M. Parizeau, C. Gagné, DEAP: Evolutionary algorithms made easy, The Journal of Machine Learning Research 13 (1) (2012) 2171–2175.

[71] P. Tsirikoglou, S. Abraham, F. Contino, Ö. Bağci, J. Vierendeels, G. Ghorbaniasl, Comparison of metaheuristics algorithms on robust design optimization of a plain-fin-tube heat exchanger, in: 18th AIAA/ISSMO Multidisciplinary Analysis and Optimization Conference, 2017, p. 3827.

[72] R. Renaldi, A. Kiprakis, D. Friedrich, An optimisation framework for thermal energy storage integration in a residential heat pump heating system, Applied energy 186 (2017) 520–529.

[73] S. M. Wilcox, National solar radiation database 1991-2010 update: User's manual, Tech. rep., National Renewable Energy Lab.(NREL), Golden, CO (United States) (2012).

[74] L. Reichenberg, F. Hedenus, M. Odenberger, F. Johnsson, The marginal system LCOE of variable renewables – Evaluating high penetration levels of wind and solar in Europe, Energy 152 (2018) 914–924.

[75] M. Hofmeister, M. Guddat, Techno-economic projections until 2050 for smaller heating and cooling technologies in the residential and tertiary sectors in the EU, Joint Research Centre (European Commission).

[76] K. K. Cao, A. N. Nitto, E. Sperber, A. Thess, Expanding the horizons of power-to-heat: Cost assessment for new space heating concepts with Wind Powered Thermal Energy Systems, Energy 164 (2018) 925–936.

[77] Vaillant, allstor exclusiv, Available online: `https://www.vaillant.be/consumenten/producten/allstor-exclusiv-2048.html`. Accessed: 22th October 2020.

[78] W. Liu, D. Klip, W. Zappa, S. Jelles, G. J. Kramer, M. van den Broek, The marginal-cost pricing for a competitive wholesale district heating market: A case study in the Netherlands, Energy 189 (2019) 116367.

[79] R. Fu, D. J. Feldman, R. M. Margolis, US solar photovoltaic system cost benchmark: Q1 2018, Tech. rep., National Renewable Energy Lab.(NREL), Golden, CO (United States) (2018).

[80] A. Allouhi, M. S. Buker, H. El-houari, A. Boharb, M. Benzakour Amine, T. Kousksou, A. Jamil, PV water pumping systems for domestic uses in remote areas: Sizing process, simulation and economic evaluation, Renewable Energy 132 (2019) 798–812.

[81] A. Kashefi Kaviani, G. H. Riahy, S. M. Kouhsari, Optimal design of a reliable hydrogen-based stand-alone wind/PV generating system, considering component outages, Renewable Energy 34 (11) (2009) 2380–2390.

[82] M. A. Ramli, A. Hiendro, S. Twaha, Economic analysis of PV/diesel hybrid system with flywheel energy storage, Renewable Energy 78 (2015) 398–405.

[83] T. H. T. Nguyen, T. Nakayama, M. Ishida, Optimal capacity design of battery and hydrogen system for the DC grid with photovoltaic power generation based on the rapid estimation of grid dependency, International Journal of Electrical Power & Energy Systems 89 (2017) 27–39.

[84] A. Khiareddine, C. B. Salah, D. Rekioua, M. F. Mimouni, Sizing methodology for hybrid photovoltaic/wind/hydrogen/battery integrated to energy management strategy for pumping system, Energy 153 (2018) 743–762.

[85] A. Singh, P. Baredar, B. Gupta, Techno-economic feasibility analysis of hydrogen fuel cell and solar photovoltaic hybrid renewable energy system for academic research building, Energy Conversion and Management 145 (2017) 398–414.